RADIATION-ABLATION COUPLING FOR CAPSULE REENTRY HEATING VIA SIMULATION and EXPANSION TUBE INVESTIGATIONS

P. Leyland*, T.J. McIntyre**, R. Morgan**, P. Jacobs **, F. Zander**, U. Sheikh**, T. Eichmann**, E. Fahy*,**, O. Joshi *, G. Duffa ***, D. Potter****, N. Banerji*, J. Mora-Monteros*, V. Marguet*

** Interdisciplinary Aerodynamics Group, GR-SCI-IAG, EPFL, CH-1015 Lausanne Switzerland,*
***Centre of Hypersonics, University Queensland, Brisbane, Australia,*
****G. Duffa, F-83 Gareoult, France*
***** DLR, Gottingen, Germany*

Abstract

A capsule entering a planetary atmosphere at hypersonic speeds experiences high levels of radiative heating. Furthermore, coupling between the ablation products from the surface of the vehicle and the high temperature gas can have a major effect on the head load experienced by the vehicle. This paper discusses a collaborative project aimed at better characterising the flow processes involved. A ground-based expansion tube facility is described in which radiation-ablation coupling is achieved through the use of a pre-heated model placed in a high temperature flow. In parallel, simulation techniques are being developed to model the complex chemical processes occurring in the flow.

1. Introduction

Capsule return missions are amongst the oldest space transportation missions dating from the Lunar exploration and subsequent return to Earth through to more recent explorations of Mars, Titan, Jupiter and Venus. One of the main features of the atmospheric entry is the extreme surface heating of the body which consists of contributions from convective and diffusive aerothermodynamic heating and from radiative heating. The design of the Thermal Protection System (TPS) of the capsule, and in particular the forebody, is highly dependent on an understanding of these heat loads. The importance of this analysis cannot be underestimated - these missions generally attempt to retrieve important scientific data or, in the case of ISS or Lunar missions, involve the return of humans to Earth.

There are several competing philosophies for the design of the TPS. One option is to use an ablative material as the heat shield on the surface of the forebody. Such designs are obligatory for hyperbolic returns, such as certain lunar return trajectories or small experimental capsules such as the recent Stardust (2006) or Hayabusa (2010) missions. The heating rates associated with these missions were so high that the exposed surface temperatures required could not be sustained continuously by any suitable existing materials, and surface erosion forms an integral part of the thermal protection mechanisms involved. However, the ablation and pyrolysing processes ejects new species into the reacting boundary layer, some of which are highly radiative, which can enhance or block the radiation heat flux.

Reproducing such trajectories and, in particular, the peak heating conditions (radiative and convective) in ground facilities is a challenging task. A high temperature flow of gas with sufficient density can generally only be created for a short period and hence such facilities are impulsive in nature with short test times. The operating conditions for the facilities are aimed to be relevant to actual missions (past, present and future) ranging from Apollo-type to sample return from Mars or Moon to small capsule missions such as Stardust, Hayabusa and ESA's recent prospective project Phoebus. Continuously running facilities such as plasma wind tunnels (PWTs) can achieve the

time dependant heat loads experienced in such missions but cannot reproduce simultaneously the flight conditions of pressure, density and enthalpy.

One type of facility that is capable of generating the flow conditions experienced during atmospheric entry is the super-orbital expansion tube. Flight conditions are created in the test section of the facility matching flow speeds, pressures, enthalpies and convective fluxes, but only for short test times of the order of 50-500 microseconds. This implies that the temperature of the surface of a model placed within the oncoming flow in the expansion tube does not reach a significant temperature as compared to flight, where the surface heats up progressively along the trajectory path reaching values of over 3000 K. However, this drawback of short testing times can be circumvented by the use of in-situ pre-heating by an electrical arc within the material [1], as long as the electrical conductivity of the material is compatible, [2]. This is the case, at least for carbon composites such as RCC and also carbon phenolics. Important information about the mechanisms involved in the ablation can be obtained by placing probes within the sample, and by the use of non-intrusive high-speed imaging and spectroscopy.

Testing of this type can be used to measure the level of radiative heat transfer from the hot radiating plasma to the surface the model. At high entry speeds this heating mechanism represents a significant contribution to the overall heat load. For a non-ablating surface, modelling of the flow chemistry can be used to infer heat flux levels. The presence of ablation significantly complicates the situation. Heat shield made from modern lightweight carbon phenolics inject highly radiating species such as CN into the hot boundary layer as well as other reacting species such as C3, C2, CO, CH, CH2, CH3, H20 and the radicals of C2H. Carbon derivatives such as CO2, CO, CN, C and C3 are mostly important for surface ablation of carbonaceous materials, whereas H, H2, CO, HCN, C2H and C3H are important for pyrolysis in the case of quasi steady-state ablation. CH3, CH4, C2H2, C2H6, H2O, H2, CO2 and CO are significant species for lower wall temperatures, especially for highly porous materials (with short time residence of gases in the material).

The ablative products interact with the radiating species of the flowfield, creating new radiating species and, in particular, the emission of products such as C3, C2, HCN, CN, CH2 and CH3 in the boundary layer enhance the radiative heat flux associated with such products and modify the transport and diffusion fluxes. Radiation blockage or a radiation enhancement can occur depending on whether the ablation and pyrolysis products are strongly absorbing or emitting. The whole procedure leads to a complex radiation-ablation coupling.

Flight data on hypervelocity entry into planetary atmospheres is extremely limited, especially with ablative coupling. In the case of Earth return, the main flight data still in use are from the Apollo era, including the FIRE II experiments and the Apollo missions themselves. The FIRE II experiment of the 60s was unique in the prediction-validation of heat flux levels and serves as a standard validation test case for International Workshops such as the ESA-CNES RHTW, Radiation Working Group and Ablation Working Group. For Apollo 4, an Avcoat5026-39G material was used which was a silica fibre/epoxy resin/phenolic microballons/silica microballons, containing also Al2O3, CaO and B2O3, and hence rendered ablative products similar to modern ablative materials. In such material the carbon deposition by pyrolysis of gases is important. Available data about this kind of material is limited and hence detailed calculation of pyrolysis and permeation of gases is difficult. [4].

Recently, small size return capsule missions have been performed. Both the Stardust and the Hayabusa missions involved super-orbital re-entry trajectories with peak values at trajectory points corresponding to altitudes of 50-58 km, rendering data from external flight path observations. It should be noted that radiative heat fluxes were approximately 10% of the total heat flux for these small sized capsules, whereas radiative fluxes are estimated to be over 40% of the total heating for certain trajectory points of FIRE II. Nevertheless, detailed measurements were made to evaluate the radiation over a large spectral range. Theoretical modelling of the missions agreed well with measurements but indicated that there was a significant contribution to the radiation from the vacuum ultraviolet (VUV) region of the spectrum which was outside the measurement capability of both the ground- and flight-testing teams.

Our consortium is conducting a project to evaluate the VUV contribution in these conditions [9]. Ground-based facilities including the super-orbital expansion tubes are being used to generate the flight conditions with observations using VUV detection systems. In parallel, numerical modelling is being conducted to compare with the measurements. This paper discusses progress in this project including the evaluation of radiation and radiation-

ablating coupling in expansion tubes, and the corresponding modelling issues related to hypervelocity return of capsules equipped with PICA-like materials.

2. Expansion tubes at UQ and Application to superorbital experiments

Researchers at the University of Queensland have developed a series of super-orbital expansion tubes capable of simulating atmospheric entry. Schematics of the X2 and X3 free-piston driven facilities, with major dimensions, can be seen in Figure 1. The X2 facility is approximately 23 metres in length with a 200 mm diameter exit flow whereas the larger X3 facility is about 65 metres long with a test flow diameter of around 600 mm. The principles and schematic of the operation of the expansion tubes is indicated in the x-t diagram also shown in Figure 1.

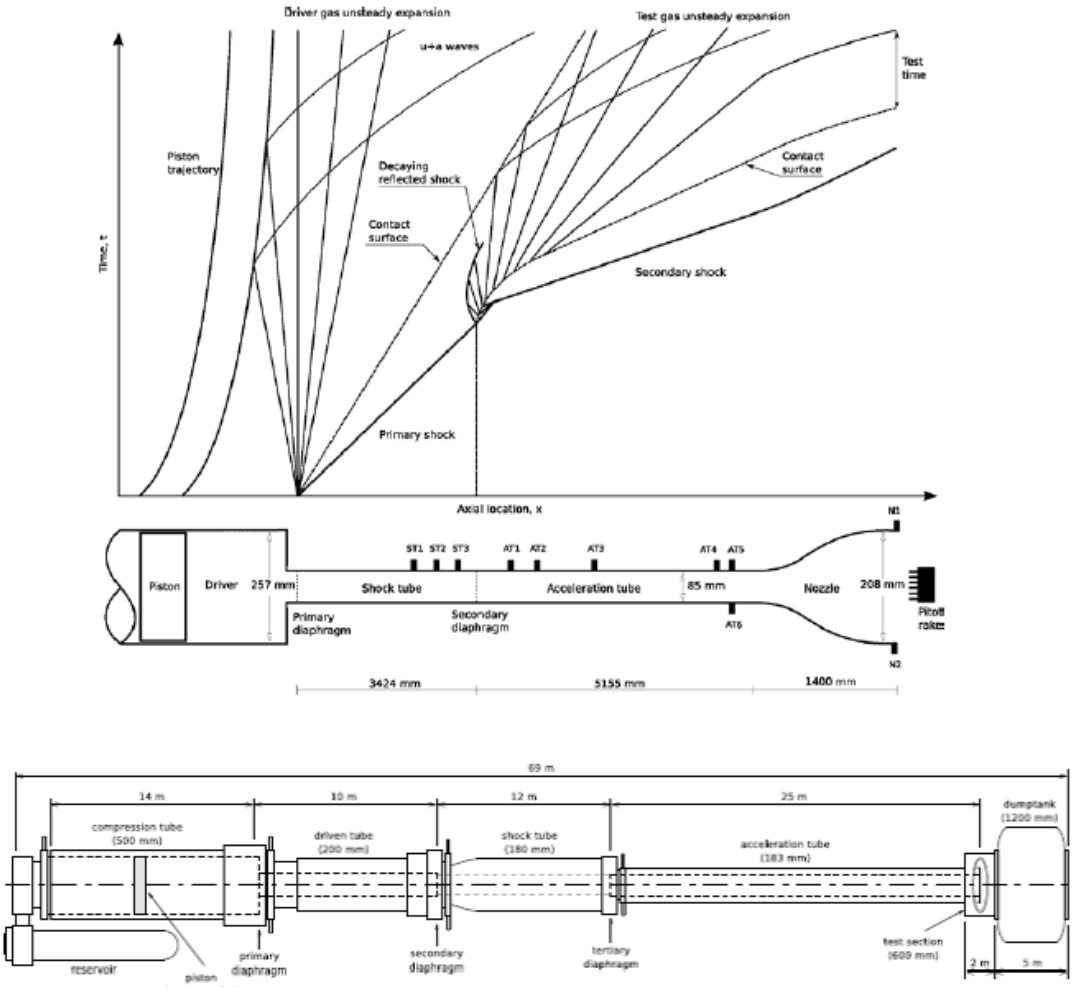

Figure 1: Expansion tube operation principles alongside schematic of X2 (mid), and dimensions of X3 (below)

The facilities can operate in either non-reflected shock tube mode NRT, or in expansion tube mode as seen in Figures 2 and 3. The first mode simulates conditions immediately behind the bow shock on a vehicle and reproduces exactly the free-stream flow speed and pressure. This allows detailed analysis of the radiation of the hot plasma and coupling with gas in the shock layer. The X2 facility in NRT mode has been used at pressures down to 4 Pa, maintaining a measurable separation between the shock and driver gas and measurements have been made using high-speed photography, pitot probes and spectrometry. In expansion tube mode, experiments can be performed on subscale models of blunt shapes such as aeroshells or material samples. The flow conditions require appropriate scaling to maintain similarity between the experiment and the true flight conditions. When the free-stream density multiplied by an appropriate length scale (so called binary scaling) is enforced as for testing in X2, there is a similarity for viscous effects and some aerothermodynamic processes such as chemical dissociation.

However, radiative energy exchange scales differently and is not fully reproduced. Nevertheless testing with expansion tube mode allows for a good representation of the non-equilibrium flow and viscous shock layer up to the surface, with reasonable testing times from a few hundred microseconds for X2 and a few milliseconds for X3. In the future we expect that the dimensions of the larger X3 nozzles will potentially allow for testing of the smaller flight vehicles like Hayabusa and Stardust to be conducted at full scale, better reproducing the true flow conditions.

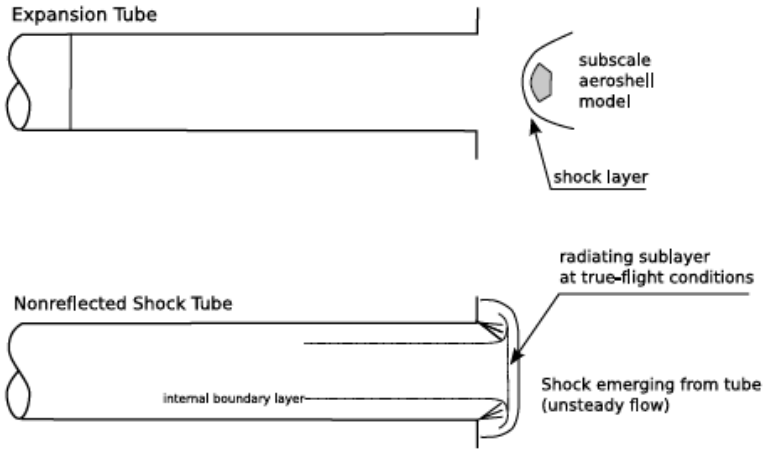

Figure 2: Operation of expansion tubes X2 and X3 for radiating and ablating flows (top) in expansion tube mode, and for radiation studies of the shock layer in Non-Reflecting-Shock tube mode (below).

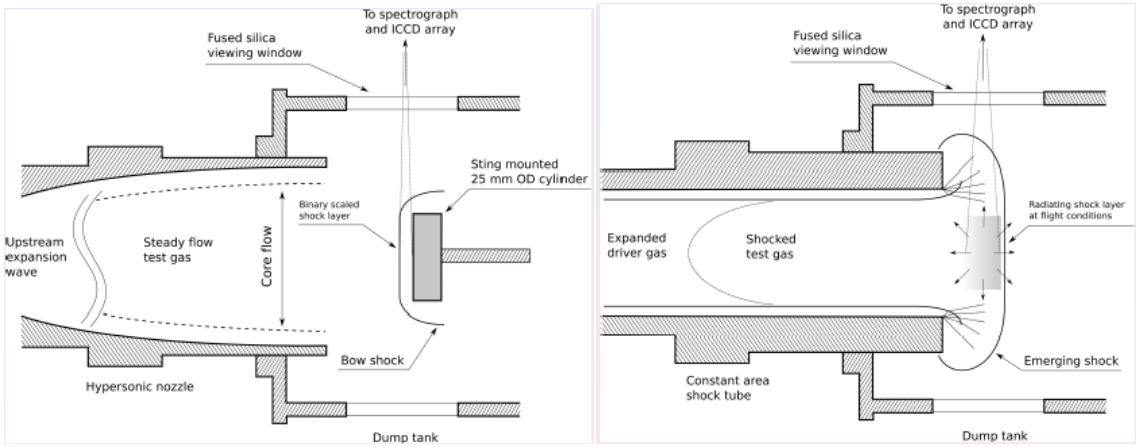

Figure 3: Close up of the zone of operation of expansion tubes X2 and X3 for radiating and ablating flows in expansion tube mode (left), and for radiation studies of the shock layer in Non-Reflecting-Shock tube mode (right).

3. Radiation-Flowfield / Radiation-Ablation Coupling

The hot plasma created by the thermal non-equilibrium dissociation levels behind the shock wave of hypervelocity (re)-entry can be characterised by the presence of highly radiating species with extensive transitions between their non-equilibrium states that radiate. A schema of the non-equilibrium processes involved is given in the Figure 4, [6]. To this is added the influence of the gas-surface interactions which depends on the material composition and possible ablation, leading to diffusion and entrainment of the ablative products into the shock layer. Some of these species are in turn highly emitting so, in addition to chemical interaction between the shock layer and the ablative products, this radiation-ablation coupling results in a complex exchange process.

It is considered as a rule of thumb that this radiation-flow-field coupling is important if local radiation energy source terms from emission and absorption are significant when compared with the flow's total energy flux through a parameter known as the Goulard Number, Γ,

$$\Gamma \sim 2 q_r / \left\{ \frac{1}{2} \rho_\infty V^3 \right\}$$

This parameter represents the ratio between the radiative flux of the shock layer to the free stream energy. If Γ is greater than approximately 0.01, it is likely that radiation coupling will be significant, and change the free stream conditions along a streamline. This ratio is also highly dependent on the trajectory path of the (re)-entry vehicle, which in turn defines the relative re-entry speeds at given altitudes/latitudes. In Figure 5, the flight profiles of typical re-entry such as Shuttle, Apollo or Mars return are represented. Trajectories of large scaled vehicles such as the Shuttle, or the ISS do not generally present conditions of high levels of radiative heat fluxes, whereas return trajectories from lunar missions (Apollo, FIRE II), Mars sample return or far solar system return present trajectory paths incurring hypervelocity trajectories with high levels of radiative surface heat flux. Also, the mass-specific enthalpy of fast return small capsules with a hyperbolic re-entry trajectory, such as the Hayabusa is double that of LEO entries as the space shuttle. For these missions the high levels of heat flux require ablative heat shields to protect the internal components from the corresponding high surface heat loads.

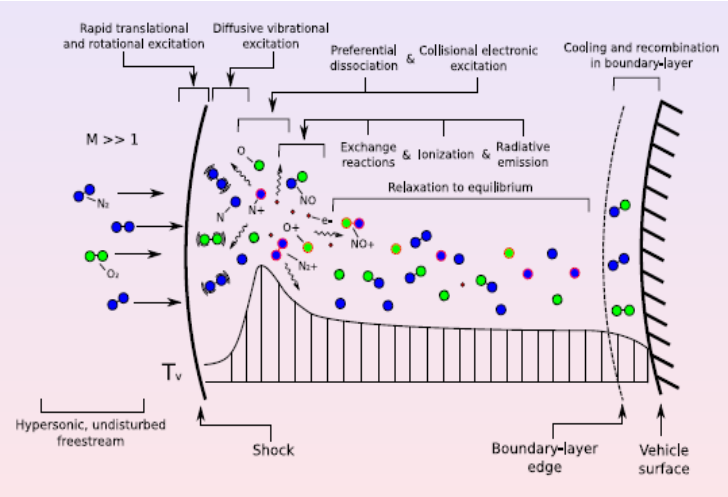

Figure 4 : Thermal non-equilibrium exchanges for hyervelocity entry situations leading to important radiation (emission and absorption) , and gas –surface interactions ; from [6].

The ejection in the boundary layer of ablation and pyrolysis products, such as hydrocarbons, hydrogen products and water include several highly radiating species that can interact with the already radiating flowfield plasma. The radiative fluxes can thus be enhanced by extra emission, or blocked by subsequent absorption. In turn, energy transport within the flowfield can be modified by the presence of significant radiative contributions, leading to enhancement or reduction of convective fluxes. Not only flowfield-radiation coupling occurs but also radiation-ablation coupling.

The level of the Goulard number is also highly dependent on the atmosphere composition and relative enthalpies rather than the entry speeds alone. Hence, entries into the Titan atmosphere such as the Huygen's probe, although at a relatively lower velocity than lunar return, (6.4 km/s), present higher radiation levels. Jupiter entry (Galileo) corresponds to speeds of about 48 km/s and post shock temperatures around 60,000 K also generating significant radiation. Apollo 4 trajectory conditions at an altitude of 120 km corresponds to a speed of 10.25km/s, a radiative intensity (over a wavelength range 0.2-4μm) of 25 $Wcm^{-2}sr^{-1}$ with a wall temperature of the order of 2500K. The recent Stardust (2006) and Hayabusa missions are small experimental half-angle sphere cone super-orbital return capsules. Hayabusa had an entry mass of 18kg, a peak convective flux about $10MW/m^2$ and a peak radiative flux of $1.85\ MW/m^2$.

Typical values of the Goulard number for these missions are approximately (at peak radiation):

- *Moon return/ FIRE II* *0.01*
- *Hayabusa* *0.013*
- *Jupiter entry* *0.1*
- *Titan entry* *0.4*

In total, radiative heat fluxes are approximately 10% of total heat flux for the small sized capsule like Stardust and Hayabusa, compared to more than 20 % for the Fire II missions, The roles of the different types of radiation, throughout the whole spectrum from VUV, UV to even far IR range are all important contributors.

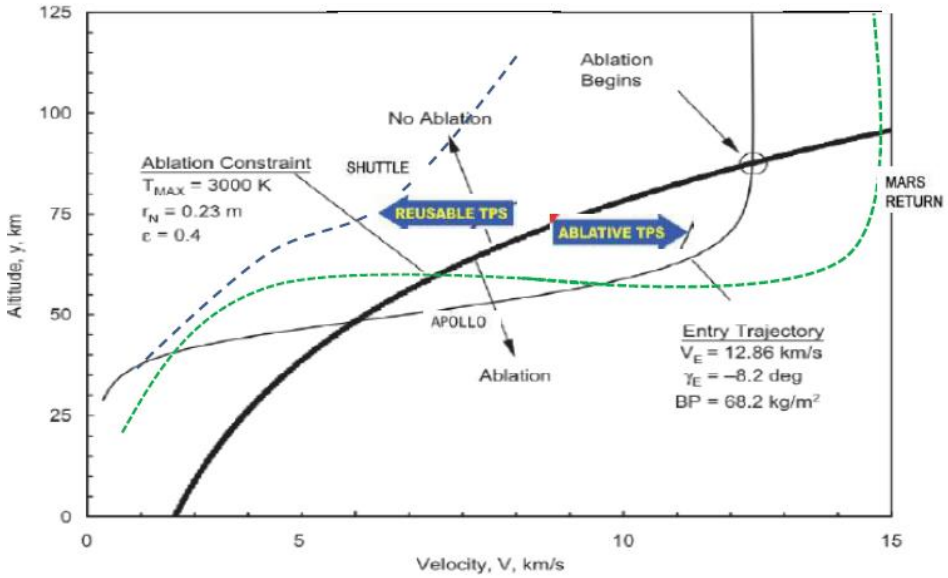

Figure 5. Earth Re-entry paths as Velocity/altitude graphs, showing the influence of the trajectories on the relative mass specific enthalpies/total pressures of entry. Shuttle type trajectories enter at high altitudes (low pressures) with moderate speeds compared to lunar or sample return. The heatflux levels from convection, diffusion, conduction and radiation lead to different requirements of Thermal Protection Systems (TPS) for the corresponding missions,(adapted from [7]).

4. Radiation and Radiation-Ablation Coupling evaluations in Expansion Tube Testing

Emission spectroscopy has been successfully implemented across the ultraviolet, visible and near infra-red parts of the spectrum in the X2 facility at the University of Queensland. This has been achieved using two spectrally sensitive camera systems – each an intensified CCD camera coupled to a spectrometer. The current systems are optimised for detection over the range 220 – 500 nm and 500 – 850 nm. Recently, a VUV spectroscopy system has been implemented [8][9]. Numerical simulations indicate that high levels of radiation can be expected in this region for super-orbital re-entry with species such as O and N contributing to the recorded spectra along with CN, CO, C and associated species in the case of surface interactions. Figure 5 shows the experimental arrangement used to record spectra from the shock layer either in front of a model in expansion tube mode or behind an incident shock in NRT mode. Testing has been completed in both configurations using X2.

A comprehensive set of shock tube experiments for a representative Huygens entry into the atmosphere of Titan (98% N2 & 2% CH4 by volume) over a pressure range of 2 to 1000 Pa and a velocity range of 4 to 10.5 km/s was conducted by Brandis [10] in the X2 facility in NRT mode. Experimental results were compared with simulations to gain insight on the radiation modelling and simulation techniques. Axisymmetric Navier–Stokes simulations were

made with the `eilmer3` (formerly `mbcns`) software developed at the University of Queensland, coupled to radiation modelling software. The Gokçen reduced chemical reaction scheme was used and a simple single temperature assumption for the thermal non-equilibrium was made. The calculated radiative intensity profiles are shown in Figure 6 along with the experimentally measured intensity profile scaled to match the order of magnitude of the one temperature simulations. The one dimensional post-shock relaxation simulation tool `poshax` is superimposed. Figure 6 shows a calculated spectrum compared to the measured spectrum, showing the distinct dominance of CN bands at 355nm, 385 nm and 415 nm. Generally good agreement is seen throughout.

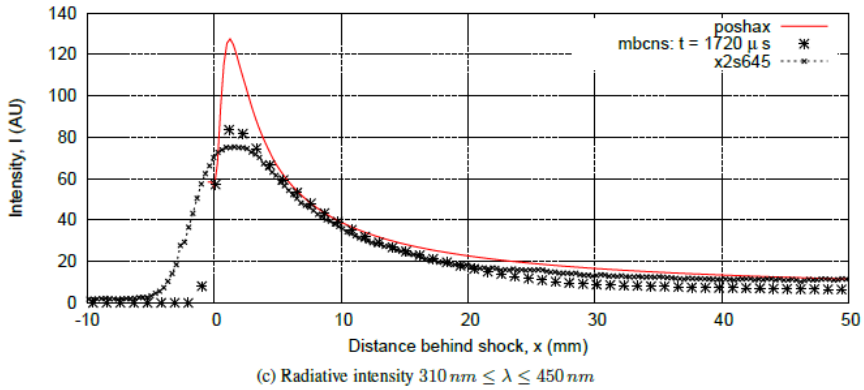

Figure 6: 1 Torr Titan condition in X2: radiative intensity between wavelengths 310 and *450 nm and comparison with one-dimensional and axisymmetric (centreline, t = 1720 μs) profiles*

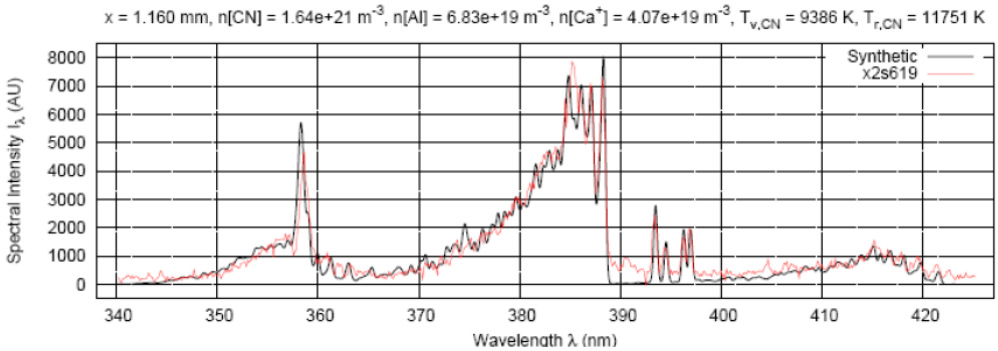

Figure 7: Fitted and measured spectra at 1.16mm from the shock front for shot x2s619 [6, 11]

The impulse facility time scales are insufficient to simulate the effects of ablation and surface chemistry on the flowfield for models initially at room temperature, which require time scales of seconds for thermal energy to be transferred into the surface and to establish representative rates of pyrolysis and mass flow which are an integral feature of the thermal response of ablative TPS in flight. Hot wall testing has been implemented in expansion tube mode using a new technique developed by Zander [1]. A resistively heated reinforced carbon-carbon (RCC) model was brought to temperatures of the order of 2000 - 3000 K in the X2 test section. The resin burns off during the pre-heating stage leaving the carbon to ablate during the test. High-speed imaging (1 MHz frame rate) was used to observe the model as it was exposed to a test flow. Small pieces of material can be seen ablating off the cylindrical model surface in the image sequence shown in Fig. 8. Experiments as part of the ESA-TRP-ARC project to investigate the radiation-ablation coupling in conditions close to the Hayabusa peak convective and peak radiation heating trajectory points are being conducted presently. The goals for future testing include developing methods to identify surface chemistry from the spectra, to determine an experimental mass flow rate due to ablation, and to extend the testing to carbon phenolic-type materials in order to achieve pyrolysis effects, as well as ablation.

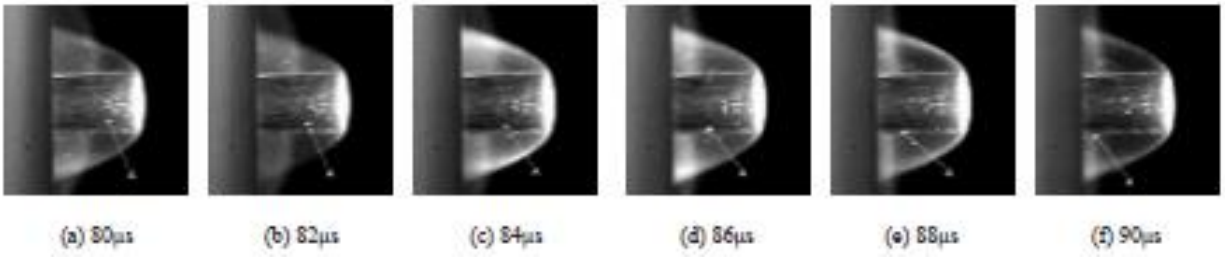

Figure 8: Images extracted from the high-speed camera footage of an ablating model; 1MHz frame rate, 0.5 μs exposure, shot x2s1758.[1]

5. Radiation and Radiation-Ablation Coupling: modelling

Modelling Equations

To study the modelling of radiation-flowfield and radiation-ablation coupling, the example of superorbital re-entry similar to Hayabusa is taken as an underlying example. The evolution of the aerothermodynamics of the flowfield is described by the compressible Navier-Stokes equations of conservation of mass, momentum and energy for a reactive gas. The thermochemical non-equilibrium is simplified by using the two-temperatures gas model formulated by Park [12], with translation-vibration exchange (Landau Teller / MillikanWhite / Park correction) T_{tv} and translation-electron exchange T_{ve}.

For simulating the flowfield, a cell-centred, finite-volume approach to the integral form of the system of the compressible Navier-Stokes equations, (2), is considered:

$$\frac{\partial \vec{U}}{\partial t} + \vec{\nabla}.(\vec{F_i} - \vec{F_v}) = \vec{Q} \tag{2}$$

With the state vector U representing mass, momentum and total energy, vibrational energy for mode m, electron-electronic energy and mass density of species s, with density ρ: $U = [\rho, \rho u, \rho E, \rho e_{vm}, \rho e_e, \rho y_s]$, the fluxes are separated into inviscid, (F_i) and viscous, (F_v) components.

For aeroshell geometries as capsule forebodies, the viscous components are calculated from the axisymmetric viscous stresses and viscous heat fluxes and the source terms, Q, is a combination of geometry, chemistry, thermal energy exchange and radiation terms. The finite volume formulation leads to the resolution of the flux balance within control volumes V:

$$\frac{\partial}{\partial t}\int_V U dV = -\oint_S \left(\overline{F}_i - \overline{F}_v\right)\cdot \hat{n}\, dA + \int_V Q dV \tag{3}$$

S represents the bounding surface and n the outward-facing normal of the control surface, A the elementary cell boundary. The vector of source terms Q is separated into geometric, chemical kinetic, thermal energy exchange and radiation contributions:

$$Q = Qgeom. + Qchem. + Qtherm. + Qrad.$$

An operator-splitting approach [13] is used to perform the time-integration. This approach decouples the inviscid and viscous gas dynamics, the thermal energy exchange and the non-equilibrium chemical kinetics and then proceeds with a loosely coupled integration in time of the ordinary differential equation (ODE) system derived from (3). A full discussion of the flux vector and source term formulations, as well as solution methods, is provided in the `eilmer3` user guide [13].

At the wall boundaries, the wall temperature can be taken as isothermal as for example the case of cold wall metallic models in expansion tubes that do not have the time to heat up due to short testing times, or based on the surface energy balance between the modes of surface heating and thermal response of the material of the wall.
The heat flux vector at the wall is composed of the components of convective and conduction heating $q_{conv,}$ the diffusion heat flux of the species q_{diff} and the total radiative heat flux q_{rad}

$$q_{total} = q_{conv} + q_{diff} + q_{rad}$$

The incident heat flux is made of a convection component, a diffusion one, and the radiative heat flux due to the radiation of the hot plasma created within the shock layer, the wall heat flux is composed of the conductive heat flux, the re-radiation heat-flux and the contributions to the surface energy balance from the ablation and pyrolysis gases (see following paragraph on ablation modelling).

Thermal non-equilibrium can be described by a multi-temperature model whereby the quantum states inside each individual energy mode (translational, rotational, vibrational, electron-electronic) are populated by a Boltzmann distribution at a common temperature for that overall mode. Single temperature (one temperature for translation, rotation, vibration and electron-electronic energy modes) formulations for hypervelocity conditions do not capture the differences in relaxation times behind the shock with enough detail. Two-temperature models are commonly implemented, with one temperature describing the translational-rotational energy modes, and one temperature to describe the vibration-electron-electronic energy modes. Vibrational-translational energy exchange is modelled by the Landau-Teller/Millikan and White empirical correlation, translation-electron exchange can be adapted from Appleton, [14] and non-preferential chemistry-energy coupling is assumed.

Finite rate non-equilibrium chemistry models describe reactions for a representation of the species that compose the atmosphere in question, as well as the ablation products and pyrolysis gases that are ejected into the flowfield and interact with the flowfield plasma when the heatshield is composed of an ablative material.

For the superorbital Hayabusa type re-entry trajectory, with an ablative heatshield, two chemistry models are selected. The first one proposed by Park 2001 [15] uses 24 reactions for 20 species: C, O, N, H, CO, C2, N2, CN, NO, O2, H2, C3, C2H, C+, O+, H+, N+, NO+, N2+, e-, and the second one was proposed by Abe [16] of 26 species, 50 reactions. A third model by Olynik [17] was also implemented, and the comparison with Park's model was reported in [2]. Park's model was derived from work of Powars and Kendall [19], for the Apollo heat shield material. It is given in the Table 1 and consists of 24 reactions: 5 dissociation reactions, 12 exchange reactions, 4 electron impact ionisation reactions, and 2 associative ionisation reactions. In this paper results will be presented using the Park's model.

Radiation modelling
Radiation modelling is performed estimating the population of the energy levels and the absorption and emission coefficients and then solving the radiative transfer equation. Two different electronic level populations models are usually considered: an equilibrium one (Boltzmann) and a non-equilibrium one (solved with QSS: Quasi Steady State). Radiation transport is performed either using the Tangent slab, Discrete transfer/Monte Carlo. As the zone behind the shock is in thermal non-equilibrium the Boltzmann does not provide enough collisions, hence a Collisional Radiative (CR) model should be used, where all excited states are considered as species.

The tangent-slab approximation, suppose that the radiation is along each line-of-sight normal to the wall. Thus the problem is reduced to the radiation of an infinitely thin parallel plane to the surface. The Discrete transfer/Monte Carlo model is based on numerical integration of the radiant energy field over direction and space. [20, 21]

Spectral radiation models were composed from several databases, as for example taking the line-by-line model for atomic and diatomic bound- bound transitions, curve fits and hydrogenic approximations for continuum transitions, electronic level and atomic line data from NIST, [22], diatomic electronic transition moments from Chauveau et al (2002)[23], details can be found in [11][24]. Electronic level populations for example for N2, $N^{+}2$, O2, N and O can be calculated by a collisional-radiative model applied in the QSS limit.

Reactions	M	C	$T_a[K]$	n	Ref.	Reactions	M	C	$T_a[K]$	n	Ref.
Dissociation reactions											
$N_2 + M \rightleftharpoons N + N + M$	All	7.0^{21}	113200	-1.6	[21]	$O_2 + M \rightleftharpoons O + O + M$	All	2.0^{21}	59360	-1.5	[21]
	C	3.0^{22}	113200	-1.6	[21]		C	1.0^{22}	59360	-1.5	[21]
	O	3.0^{22}	113200	-1.6	[21]		O	1.0^{22}	59360	-1.5	[21]
	N	3.0^{22}	113200	-1.6	[21]		N	1.0^{22}	59360	-1.5	[21]
	H	3.0^{22}	113200	-1.6	[21]		H	1.0^{22}	59360	-1.5	[21]
	e^-	3.0^{24}	113200	-1.6	[21]	$H_2 + M \rightleftharpoons H + H + M$	All	2.2^{14}	48300	0.0	[21]
$C_2 + M \rightleftharpoons C + C + M$	All	3.7^{14}	69900	0.0	[21]		H_2	5.5^{14}	48300	0.0	[21]
$CN + M \rightleftharpoons C + N + M$	All	2.5^{14}	87740	0.0	[21]						
Neutral exchange reactions											
$N_2 + O \rightleftharpoons NO + N$	–	5.7^{12}	42938	0.42	[21]	$CN + O \rightleftharpoons NO + C$	–	1.6^{13}	14600	0.10	[21]
$NO + O \rightleftharpoons O_2 + N$	–	8.4^{12}	19400	0.0	[21]	$CN + C \rightleftharpoons C_2 + N$	–	5.0^{13}	13000	0.0	[21]
$CO + C \rightleftharpoons C_2 + O$	–	2.0^{17}	58000	-1.0	[21]	$CO + C_2 \rightleftharpoons C_3 + O$	–	1.0^{12}	41200	0.0	[21]
$CO + O \rightleftharpoons O_2 + C$	–	3.9^{13}	69200	-0.18	[21]	$C_3 + N \rightleftharpoons CN + C_2$	–	1.0^{12}	34200	0.0	[21]
$CO + N \rightleftharpoons CN + O$	–	1.0^{14}	38600	0.0	[21]	$C_3 + C \rightleftharpoons C_2 + C_2$	–	1.0^{12}	16400	0.0	[21]
$N_2 + C \rightleftharpoons CN + N$	–	1.1^{14}	23200	-0.11	[21]	$C_2H + H \rightleftharpoons C_2 + H_2$	–	1.0^{12}	16770	0.0	[21]
Electron impact ionization reactions											
$O + e^- \rightleftharpoons O^+ + e^- + e^-$	–	3.9^{33}	158500	-3.78	[21]	$C + e^- \rightleftharpoons C^+ + e^- + e^-$	–	3.7^{31}	130720	-3.00	[21]
$N + e^- \rightleftharpoons N^+ + e^- + e^-$	–	2.5^{34}	168200	-3.82	[21]	$H + e^- \rightleftharpoons H^+ + e^- + e^-$	–	2.2^{30}	157800	-2.80	[21]
Associative ionization reactions											
$N + O \rightleftharpoons NO^+ + e^-$	–	5.3^{12}	31900	0.0	[21]	$N + N \rightleftharpoons N_2^+ + e^-$	–	4.4^{7}	67500	1.5	[21]

Table 1:Chemical reactions for Park's model for air chemistry with ablation (2001)

Ablation modelling

The severe thermochemical re-entry conditions for probes such as Hayabusa requires the use of ablative materials such as a carbon-phenolic TPS. The high heat loads induce an important increase in temperature inside the material which strongly modifies the ablator through essentially two different physical processes: pyrolysis and ablation. Pyrolysis is the high temperature induced reaction that transforms the pyrolysing component of the polymer matrix into gas. This gas reaches the fluid/solid interface as it is free to move toward the porous structure and is injected in the boundary layer depending on in-depth pressure and temperature gradient. Ablation consists in the decomposition of the material structure due to heterogeneous chemical reactions such as oxidation and nitridation, phase changes such as sublimation or mechanical erosion like spallation. A scheme of TPS decomposition is shown here:

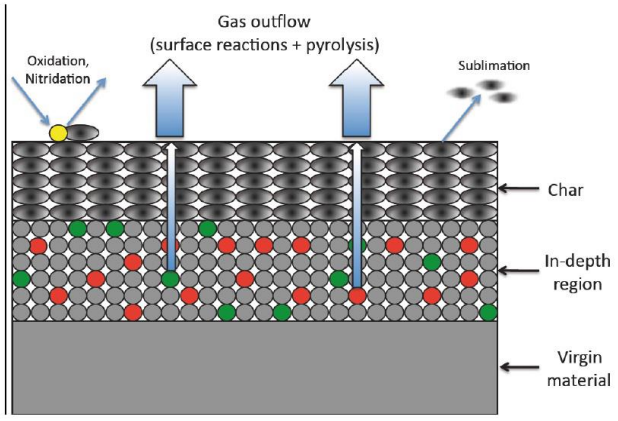

Figure 9: Processes of decomposition of an ablator under high heat loads

Modelling of ablation and pyrolysis can be reduced to the development of equivalent boundary conditions following the conservation of mass, momentum and energy across the surface, as depicted in equations and figure 10.

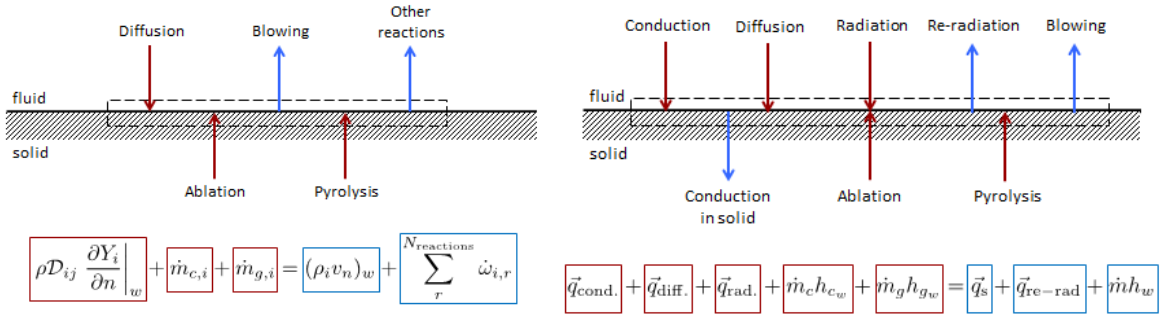

$$\rho \mathcal{D}_{ij} \left.\frac{\partial Y_i}{\partial n}\right|_w + \dot{m}_{c,i} + \dot{m}_{g,i} = (\rho_i v_n)_w + \sum_r^{N_{\text{reactions}}} \dot{\omega}_{i,r} \qquad \vec{q}_{\text{cond.}} + \vec{q}_{\text{diff.}} + \vec{q}_{\text{rad.}} + \dot{m}_c h_{c_w} + \dot{m}_g h_{g_w} = \vec{q}_s + \vec{q}_{\text{re-rad}} + \dot{m} h_w \quad (10)$$

Figure 10: Equations of Surface mass balance and Energy balance [18]

where the mass blowing rate has two components: $\dot{m}_c$ due to the char and $\dot{m}_g$ due to the pyrolysis gases. $\omega_{i,r}$ corresponds to the mass production of species i during surface reaction r. At the interface, mass fluxes are flowing out from blowing and chemical reactions (blue) while other mass fluxes are entering the solid domain due to diffusion, injection of ablation species and injection of pyrolysis gases. On the right hand equation in figure 10 the energy flux balances between entering and leaving energy fluxes are given. Blowing energies are computed by multiplying the mass flow rate $\dot{m}_i$ by the enthalpy h_i.

To describe the thermal response due to the effects of heat flux on the material, heating, pyrolysis of phenolic resin and gas migration through the porosity up to the point where it 'blows' into boundary layer have to be considered. For this purpose a code named SACRAM was developed using the assumption of chemical equilibrium between the pyrolysis gases and the char gases. This hypothesis is lifted at surface where the composition of pyrolysis gases is done by minimisation of the free enthalpy. This code was verified by comparison to available data of a generic carbon phenolic material TACOT published in NASA ablation workshop, [25]. The discretisation on a moving grid allows taking into account the surface ablation. This code was coupled to the CFD code eilmer3 by a partitioned method as depicted in the figure 12, [18]

The technique in SACRAM uses a CVFEM spatial discretisation, with a contracting grid, and an implicit Euler time integration with a Newton non-linear solver, [26],[18].

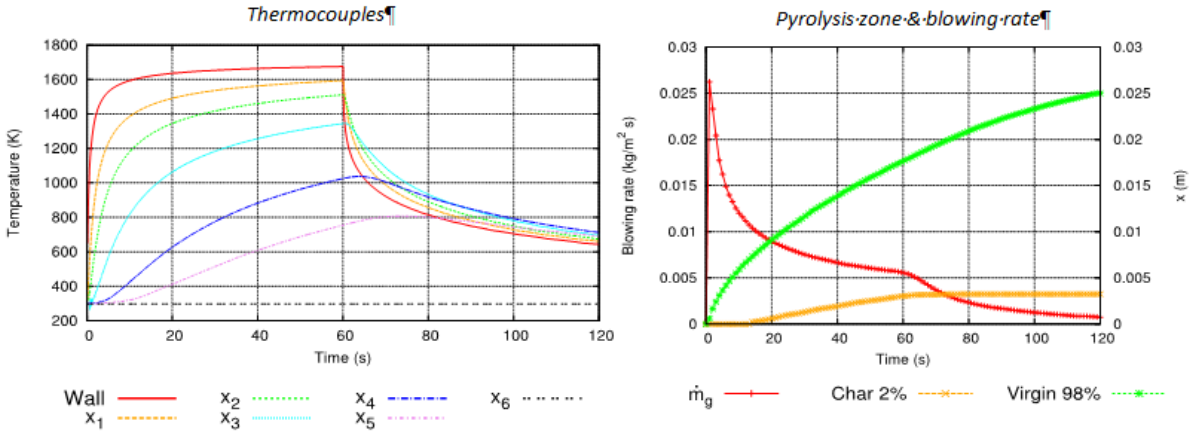

Figure 11: NASA Ablation Workshop Test Case 2 results obtained using sacram*: Left: temperature histories for all thermocouples distributed in-depth of the test slab. Right: histories for surface mass blowing rate (left axis, red curve), location of pyrolysis front (Virgin 98%, green curve) and location of charred material front (Char 2%, orange curve).*

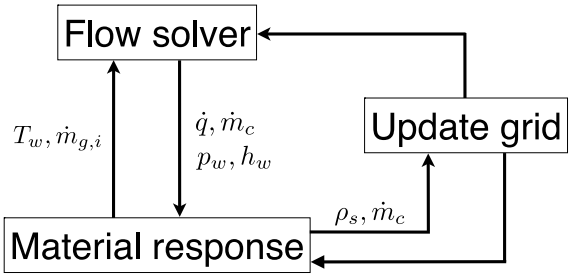

Figure 12: Ablation code – Flowfield aerochemistry coupling

Results

The results are presented for a prospective ESA mission Phoebus which is similar to Hayabusa, and whose peak heating trajectory points are similar. It is a passive 45 deg sphere cone with a base diameter of 510 mm and an approximate mass of 25 kg, and enters at a slightly lower velocity than Hayabusa (10.5 km/s compared to 11.8km/s).

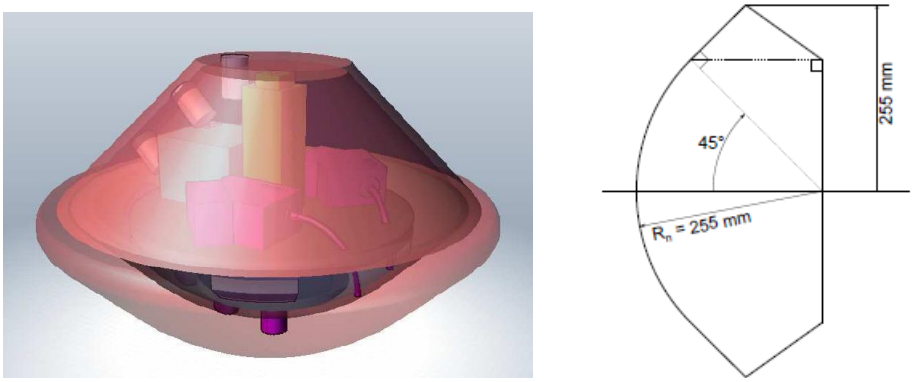

Figure 13: Form and Dimensions of the Phoebus Capsule

Four trajectory points are retained:
TP1 corresponds to a low pressure (high altitude) at stagnation point, TP2 corresponds to the maximum radiative heat flux, TP3 corresponds to the maximum convective heat flux and TP4 correspond to a high pressure at stagnation point:

Name	Time	Altitude	ρ_∞ (kg/m^3)	T_∞ (K)	p_∞ (Pa)	u_∞ (m/s)	Mach
TP1	18.4	64981	1.64e-4	233.3	10.96	10916	35.65
TP2	21.8	55449	4.23e-4	254.0	30.96	10044	32.04
TP3	24.1	49464	1.10e-3	270.6	85.28	9518	28.86
TP4	26.0	45004	2.00e-3	264.2	149.10	8456	25.95

Table 2: Trajectory points for hyperbolic entry of a superorbital probe project Phoebus.

Flow simulations are steady-state calculations at multiple points of the discretised trajectory, while the material response is time-accurate for the whole trajectory time. For this reason, boundary conditions that are imposed to SACRAM must be interpolated between two successive trajectory points. Since the material response code is 1D, SACRAM is run for each point of the capsule surface and surface temperature Tw and pyrolysis injection rates $\dot{m}_g$ are obtained. Pyrolysis gas is assumed to be in chemical equilibrium and its composition at surface temperature is calculated by an in-house chemical reaction tool that minimises the Gibb's free energy; this step can alternatively be replaced by using CEA for example. This allows to estimate the species concentration at the wall, $\dot{m}_{g,i}$. The finite rate chemistry ablation boundary condition is used to calculate $\dot{m}_c$ and the consequent state of the boundary layer

and the incident heat fluxes on the wall. The new geometry and mesh is updated and the computational cycle repeated. The whole procedure is iterative.

The model of Park of 20 species and 24 reactions (Table 1) contains

- 10 air species: O, N, N_2, NO, O_2, O+, N+, NO+, N_2+, e-
- 10 ablation species: C, H, H_2, C_2H, CO, C_2, CN, C_3, C+, H+

The mesh is optimised and highly refined mesh close to wall, and the calculations were performed in 2D axisymmetric mode. The material properties from NASA TACOT test case which describes a generic carbon phenolic resin (C_6H_5OH). This reacts with the thermal non-equilibrium air of which some main heterogeneous reactions are

- Oxidation by monoatomic oxygen: O(g) + C(s)) →CO(g),
- Oxidation by diatomic oxygen: O2(g) + 2C(s)) →2CO(g),
- Nitration by dissociated nitrogen: N(g) + C(s)) →CN(g)
- Sublimation/deposition: 3C(s) → C3(g).

As for example in the Figure 14, where a more complete model of PICA is presented:

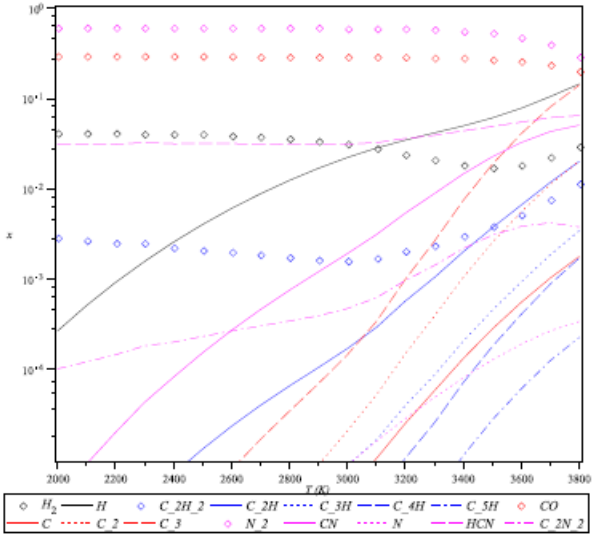

Figure 14: Typical wall composition for a carbon-resin composite in thermodynamic equilibrium [27]

The radiation was also accounted for using a tangent slab approximation was used to estimate the radiative fluxes, using a detailed spectroscopic database between 50 and 2000 nm that is a mixture of existing data and implemented as a library in `eilmer3`.

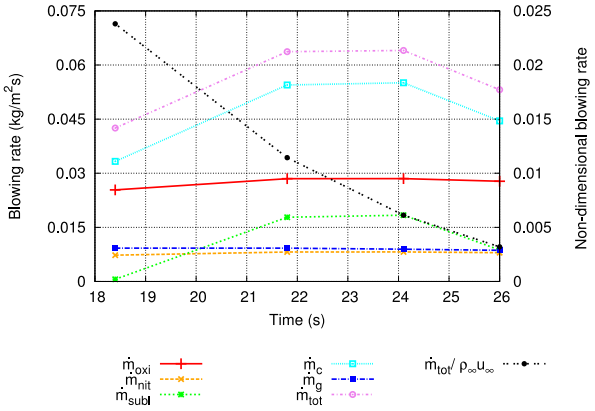

Figure 15: Composition of non-dimensional mass blowing rates at stagnation point for the Phoebus re-entry trajectory.(TP1 to TP4) ; The components of the total mass blowing rate are surface ablation products blowing rates (oxidation, nitridation and sublimation) calculated by finite chemistry reactions at the surface [29] and pyrolysis gas injection.

Figure 15 gives the part of each phenomenon in the creation of species at wall. The oxidation is the dominant effect giving abundant CO. Then the sublimation is the second ablating phenomenon resulting in the presence of C (mainly) and C_3. The last effect is due to pyrolysis with the presence of molecular and atomic hydrogen. The non-dimensional blowing rate gives an indication of the importance of the mass injection at the wall with respect to the free stream conditions.

The coupled calculations allow to obtain the species present in the flow (figure 9.10). The results are presented for the peak convective heating trajectory point TP3: the fact of only considering the pyrolysis gas mass flow rate, the concentrations of ablative species at the wall are low as compared to the more complete model in Figure 14 above.

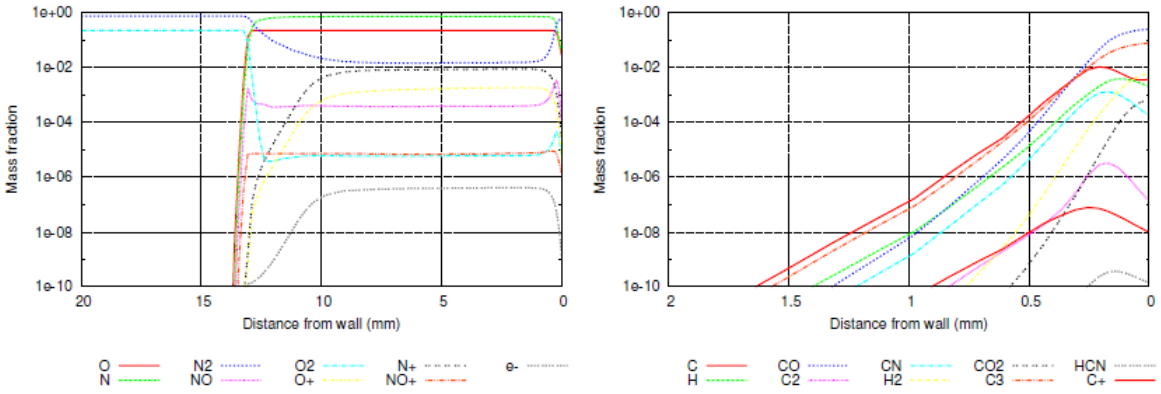

Figure 16: Coupled simulations results: TP3 mass fractions of air (left) and ablative species (right) along the stagnation streamline using Park's 20 species 24 reactions model.

The rate of dissociation of N2 and O2 molecules lowers during the re-entry, up to the point that N2 amounts to 17% of the flow gases with Park's model. Monoatomic N recombines almost completely into N2 at the wall.
Evolution of ablative species are also presented on the right hand side of Figure 16: As the capsule descends and the density of the outer flow increases, pyrolysis and ablation gases find a greater resistance to penetrate into the boundary layer, with the significant diffusion going from over 1.5mm from the wall of TP1 to a little over 1mm of TP4.

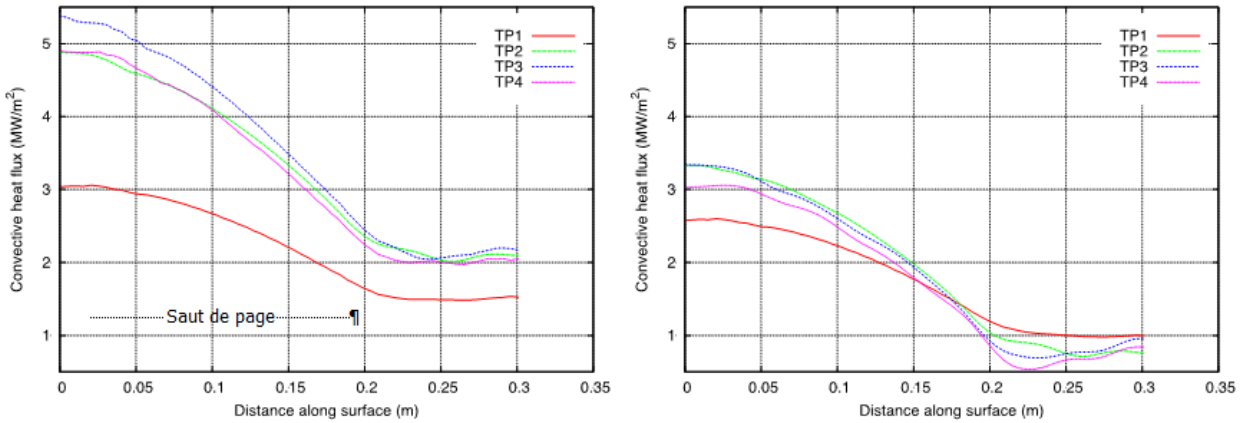

Figure 17: Heating along the capsule at maximum convective heating Trajectory Point TP3

In Figure 17 the heating along the capsule body from stagnation to the shoulder is presented showing that ablation reduces convective heat fluxes by 20-25%.

Radiation heat flux profiles are obtained using a Boltzmann distribution for populating energy levels when there is thermal equilibrium (this is almost the case for TP3) and a collisional radiative model using QSS approximation when considering thermal non-equilibrium (TP1, TP2 and TP4). In all four cases, there is a noticeable difference

between the two population models. The Boltzmann approximation over-predicts the radiative heat flux by at least 25% with respect to QSS simulation results for TP1 to 3.

Radiative heat flux is noticed to be smaller with ablation than without where CN is present in small amount, the radiative flux which is reduced by the presence of ablation products due to the increased absorption in the boundary layer due to the presence of these species. This radiation blockage effect is not as well understood as the blowing correction and is under study at the present time. This is in agreement with the study of Johnston [28].

	Ablation		No-ablation	
	Boltzmann	QSS	Boltzmann	QSS
TP1	$1.43\,\mathrm{MW\,m^{-2}}$	$1.26\,\mathrm{MW\,m^{-2}}$	$1.72\,\mathrm{MW\,m^{-2}}$	$1.54\,\mathrm{MW\,m^{-2}}$
TP2	$1.60\,\mathrm{MW\,m^{-2}}$	$1.45\,\mathrm{MW\,m^{-2}}$	$1.81\,\mathrm{MW\,m^{-2}}$	$1.64\,\mathrm{MW\,m^{-2}}$
TP3	$1.29\,\mathrm{MW\,m^{-2}}$	$1.19\,\mathrm{MW\,m^{-2}}$	$1.38\,\mathrm{MW\,m^{-2}}$	$1.29\,\mathrm{MW\,m^{-2}}$
TP4	$1.09\,\mathrm{MW\,m^{-2}}$	$1.02\,\mathrm{MW\,m^{-2}}$	$1.16\,\mathrm{MW\,m^{-2}}$	$1.10\,\mathrm{MW\,m^{-2}}$

Table 3: Comparison of radiative heat flux levels.

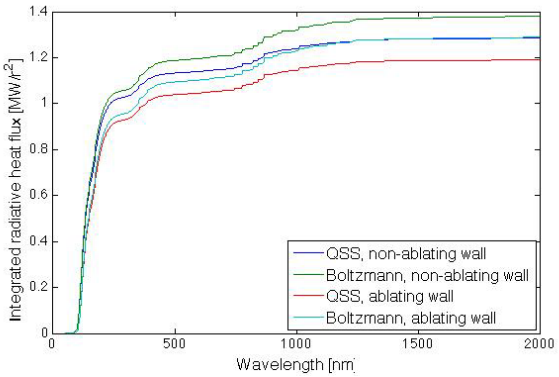

Figure18: Integrated radiative heat fluxes at TP3.

Finally it is interesting to note that from these theoretical estimations, as well as in the literature, about 75 % of the radiative heat flux is within the VUV range (50-200 nm) and the importance of VUV almost the same with and without ablation. This is under study experimentally within an ESA TRP study on going at present.

Conclusions

Although capsule technology dates from the early 60s and the space exploration race, they remain and will continue, to be significant space exploration shapes for their versatile large radius heatshield for dissipating energy for hypervelocity entry or return. Advances in research are being made on the coupling of the heat loads to the capsule TPS, in particular when this is made of an ablating material of composites, such as Carbon matrix/Carbon phenolics or Si-C shells with resins. In this paper we have discussed testing of scaled to almost flight models in expansion tubes at near flight conditions, and ablation modelling. The new possibilities of performing in-situ heating of samples in expansion tubes open many interesting perspectives for validation of modelling activities on radiation-ablation coupling.

Acknowledgements

The work related in this paper was partially supported by Australian Research Council grant numbers DP1094560 and DP120102663 and the Queensland Government Smart State Scheme, as well as by the European Space

Agency's ESA-TRP AMOD, ESA-TRP-ARC, ESA NPI fellowship scheme, Swiss National Research Foundation, SNF grants numbers 200021_146710, 200021_140701, and 200021_140695.

References

1. F. Zander, R. G. Morgan, U. Sheikh, D. R. Buttsworth, P. R. Teakle; *Hot wall reentry testing in hypersonic impulse facilities.* AIAA Journal, Vol 51, No. 2, pp. 476-484, 2013.
2. O. Joshi, J. Mora-Monteros, P. Leyland; *Ablation Radiation Coupling of the Phoebus Capsule.* In Proceedings 5th RHTG ESA-CNES-ERCOFTAC Workshop, Barcelona 2012, ESA SP714.
3. P. Jacobs, R. Morgan, et al, D*esign, Operation and Testing in Expansion Tube Facilities for Super-Orbital Re-entry.* VKI-LS 2013.
4. Park, C. *Stagnation-Point Radiation for Apollo 4*. Journal of Thermophysics and Heat Transfer 18 (2004), 349–357.
5. U.A Sheikh, C. Jacobs, C.O Laux, R.G Morgan, and T.J McIntyre, *Measurements of Radiating Flow Fields in the Vacuum Ultraviolet and Ultraviolet Emission*; 29th International Symposium on Shock Waves, July 14-19 in Madison, WI.
6. R. Savajano, D. Potter, P. Leyland; *Radiation Master Model,* TN 7.2, AMOD TRP-ESA, 2010.
7. T. Rivell et al. *NASA TP-21348, 2006*
8. Umar A Sheikh, Richard G Morgan, Timothy J McIntyre; *Self-absorption of Vacuum Ultraviolet radiation in superorbital flows;* ESA Publications SP714 2012 and
   Sheikh, U., Morgan, R. Zander, F., Eichmann, T., McIntyre, T.J.; *Vacuum Ultraviolet Emission Spectroscopy System for Superorbital Reentries.* 18th AIAA/3AF International Space Planes and Hypersonic Systems and Technologies Conference, Tours, France, 2012
9. P. Leyland T. McIntyre, U. Sheikh T. Eichmann, F. Zander, R. Morgan ; S. Loehle F. Defillippis, E. Trifoni; *VUV measurements for radiation-ablation coupling*. Proceedings 5th International Symposium on Radiation of High Temperature Plasmas, RHTW, Barcelona October 2012. ESA Publications SP714 2012.
10. A. Brandis; PhD, Thesis, Centre of Hypersonics, University of Queensland. *Experimental study and modelling of non-equilibrium radiation during Titan and Martian entry.* 2009.
11. D. Potter; PhD Thesis University of Queensland, *Modelling of radiating shock layers for atmospheric entry at Earth and Mars,* 2011.
12. C. Park; *Nonequilibrium Hypersonic Aerothermodynamics*. Wiley-Interscience, 1990
13. P.A. Jacobs, R. J. Gollan; The Eilmer3 code: User guide and example book. Mechanical Engineering Report 2008/07, The University of Queensland, Brisbane, Australia, 2010.
14. J.P. Appleton and K.N.C. Bray; *"The conservation equations for a nonequilibrium plasma"*. Journal of Fluid Mechanics, 20(4):659 - 672, December 1964.
15. C. Park, R. Jaffe, H. Partridge; *Chemical Kinetic Parameters of Hyperbolic Earth Entry*, Journal of Thermophysics and Heat Transfer, Vol. 15, No. 1, 2001, pp; 76-90
16. Takashi Abe; *Overview of research for prediction of aerodynamic heating environment during a super-orbital reentry flight of muses-c reentry capsule.* In Aerodynamics, Thermophysics, Thermal Protection, volume 1, page 19, 2003.
17. Olynick, Y.-K. Chen, M. E. Tauber; *Aerothermodynamics od the Stardust Sample Return Capsule,* Journal of Spacecraft and Rockets, Vol. 36, No. 3, May 1999, pp. 442-462
18. *O. Joshi, Fluid-Structure Thermal Coupling and Ablation Effects in Atmospheric Entry, PhD Thesis of Ecole Polytechnique Fédérale de Lausanne, May 2013.*
19. C. Powars and R. Kendall; User's manual, aerotherm chemical equilibrium (ace) computer program. Aerotherm Corp., May, 1969
20. S. Karl; *Simulation of Radiative Effects in Plasma Flows*. DC report, von Karman Institute for Fluid Dynamics. 2001
21. Potter, D. and Karl S; 2009. *Validation of aerothermo-chemistry models for re-entry application. TN 3.2: Engineering models for radiation*. AMOD ESA TRP Technical Note 3.2, European Space Agency, Noordwijk, The Netherlands.
22. NIST Chemical Kinetics Database, Ver. 7.0, 2003
23. Chauveau et al.; *Radiative transfer in LTE air plasmas for temperatures up to 15,000 K*. Journal of Quantitative Spectroscopy and Radiative Transfer 77, 2 (March), 113–130. 2003

24. R. Savajano. PhD Thesis EPFL, *Aerochemistry and Radiation flowfield coupling for Erath Re-entry and Titan entry*, August 2013.
25. NASA ablation workshop, Lexington, Kentucky, 2012.
26. A. J. Amar, B. F. Blackwell, and J. R. Edwards. *One-dimensional ablation using a full newton's method and finite control volume procedure.* Journal of Thermophysics and Heat Transfer, 22(1), 2008.
27. G. Duffa; "*Modelisation des Systèmes de Protections Thermiques Ablatives".* Book, to appear AIAA Educational Series 2013 under the title "*Ablative Thermal Protection Systems Modeling"*. Also in ESA SP-714. 2012
28. C. O. Johnston, P. A. Gnoffo, K. Sutton; *The Influence of Ablation on Radiative Heating for Earth Entry*, Journal of Spacecraft and Rockets, Vol. 46, No. 3, June 2009, pp. 481-49
29. A. Haemmerle; "*Conditions d'interactions gaz-surface en presence d'ablation*", GR-SCI-IAG Report, 2011.